Experimental and Kinetic Modeling Study of C_2H_2 Oxidation at High Pressure

Jorge Gimenez Lopez[1,2], Christian Tihic Rasmussen[1], Hamid Hashemi[1], Maria U. Alzueta[2], Yide Gao[3], Paul Marshall[3], C. Franklin Goldsmith[4], and Peter Glarborg[1]

[1]*Department of Chemical and Biochemical Engineering, Technical University of Denmark, DK-2800 Kgs. Lyngby, Denmark*

[2]*Department of Chemical and Environmental Engineering, University of Zaragoza, 50018 Zaragoza, Spain*

[3]*Department of Chemistry and Center for Advanced Scientific Computing and Modeling, University of North Texas, 1155 Union Circle #305070, Denton, Texas 76203-5017*

[4]*School of Engineering, Brown University, Providence, Rhode Island 02912, United States*

A detailed chemical kinetic model for oxidation of acetylene at intermediate temperatures and high pressure has been developed and evaluated experimentally. The rate coefficients for the reactions of C_2H_2 with HO_2 and O_2 were investigated, based on the recent analysis of the potential energy diagram for $C_2H_3 + O_2$ by Goldsmith et al. and on new ab initio calculations, respectively. The $C_2H_2 + HO_2$ reaction involves nine pressure and temperature dependent product channels, with formation of triplet CHCHO being dominant under most conditions. The barrier to reaction for $C_2H_2 + O_2$ was found to be more than 50 kcal mol^{-1} and predictions of the initiation temperature were not sensitive to this reaction. Experiments were conducted

with C_2H_2/O_2 mixtures highly diluted in N_2 in a high pressure flow reactor at 600–900 K and 60 bar, varying the reaction stoichiometry from very lean to fuel-rich conditions. Model predictions were generally in satisfactory agreement with the experimental data. Under the investigated conditions the oxidation pathways for C_2H_2 are more complex than those prevailing at higher temperatures and lower pressures. Acetylene is mostly consumed by recombination with H to form vinyl (reducing conditions) or with OH to form a CHCHOH adduct (stoichiometric to lean conditions). Both C_2H_3 and CHCHOH then react primarily with O_2. The CHCHOH + O_2 reaction leads to formation of significant amounts of glyoxal (OCHCHO) and formic acid (HOCHO), and the oxidation chemistry of these intermediates is important for the overall reaction.

Introduction

Acetylene (C_2H_2) is an important intermediate in combustion of hydrocarbons and a precursor of PAH and soot. Previous studies of C_2H_2 oxidation have been conducted in static reactors [1–4], jet-stirred reactors [5], flow reactors [6], shock tubes [7–14], and premixed laminar flames [15–32]. Comprehensive modeling studies of acetylene oxidation have been published by Tan et al. [5] and by Lindstedt and Skevis [33]. Even though these studies cover a fairly wide range of stoichiometries and temperatures, results for the low-to-medium temperature oxidation chemistry of acetylene is limited to the early static reactor work [1–4], and the few experiments conducted at increased pressure [5, 14, 32] are limited to pressures up to 20 bar.

The objective of the present study is to develop and evaluate a detailed chemical kinetic model for oxidation of acetylene at high pressure and intermediate temperatures. The model draws on previous work on the high-pressure, medium temperature oxidation of small hydrocarbons and alcohols [34–40], as well as recent results in atmospheric chemistry. The rate constants for the reactions of acetylene with HO_2 and O_2 are investigated from theory. Experimental data are obtained in a flow reactor for oxidation of C_2H_2 at high pressure (50–60 bar) as a function of temperature (600–900 K) and stoichiometry (lean to fuel-rich). Modeling predictions are in satisfactory agreement with the flow reactor results. The oxidation pathways for C_2H_2 under these conditions are different from those prevailing at higher temperatures and lower pressures and the results of the current work help to extend the validation range for chemical kinetic modeling of C_2H_2 oxidation. In addition to the present data, predictions are compared to selected experimental data from the literature on ignition delays and flame speeds.

Experimental

The experimental setup is a laboratory-scale high-pressure laminar flow reactor designed to approximate plug-flow. The setup is described in detail elsewhere [35] and only a brief description is provided here. The system enables well-defined investigations of homogeneous gas phase chemistry at pressures from 10 to 100 bar, temperatures up to 925 K, and flow rates of 1–5 L min^{-1} (STP). The reactions take place in a tubular quartz reactor, enclosed in a stainless steel tube that acts as a pressure shell. The steel tube is placed in a tube oven with three individually controlled electrical heating

elements that produce an isothermal reaction zone (±5 K) of 43 cm. The reactor temperature is monitored by type K thermo-couples (±2.2 K or 0.75 %) positioned in the void between the quartz reactor and the steel shell. The heat of reaction introduces some uncertainty in the temperature but due to high dilution of reactants it is below 20 K.

The reactant gases are premixed before entering the reactor. All gases used in the experiments are high purity gases or mixtures with certified concentrations (±2% uncertainty). The system is pressurized from the feed gas cylinders. Downstream of the reactor, the system pressure is reduced to atmospheric level prior to product analysis, which is conducted by an on-line 6890N Agilent Gas Chromatograph (GC-TCD/FID from Agilent Technologies). The GC allows detection of O_2, CO, CO_2, C_2H_6, C_2H_4, C_2H_2, and CH_4 with an overall relative measuring uncertainty in the range ±6%. For comparisons with modeling predictions, it should be noted that these uncertainties are minor compared to those associated with the temperature profiles.

Experimental data are obtained as mole fractions as a function of the reactor temperature measured at intervals of 25 K. The reactor operates in the laminar flow regime, but under conditions tailored to approximate plug flow [35].

Theory

The ignition delay time and the temperature for onset of reaction in oxidation of acetylene at high pressure and medium to low temperature may

be sensitive to the reaction of acetylene with oxygen, which is believed to be an important initiation step, and to the C_2H_2 + HO_2 reaction, because the HO_2 radical achieves considerable concentrations under these conditions. The rate constants of these two steps are discussed further below, based on theory.

Reaction of C_2H_2 with HO_2

The rate constant for the reaction of C_2H_2 with the hydroperoxy radical HO_2 has not been determined experimentally; only a room temperature upper limit of $3 \cdot 10^9$ cm^3 mol^{-1} s^{-1} has been reported [41]. In earlier modeling studies, estimates of $1 \cdot 10^{12}$ exp(-5030/T) cm^3 mol^{-1} s^{-1} for product channels to CH_2HCO + O and CH_2O + HCO, respectively, have been employed [42]. These estimates are in agreement with the room temperature upper limit, but both the rate constant and the product composition are uncertain.

The addition of HO_2 to C_2H_2 can result in several distinct products, as shown in Fig. 1. Of the eight possible unimolecular products, only CH_2CHOO is formed under combustion conditions, and even then only at the highest pressures. The most significant product channels are:

$$C_2H_2 + HO_2 \rightleftarrows {}^3CHCHO + OH \quad \text{(R12)}$$

$$C_2H_2 + HO_2 \rightleftarrows CH_2CHO + O \quad \text{(R13)}$$

$$C_2H_2 + HO_2 \rightleftarrows C_2H_3 + O_2$$

$$C_2H_2 + HO_2 \rightleftarrows OCHCHO + H \quad \text{(R14)}$$

$$C_2H_2 + HO_2 \rightleftarrows CH_2CO + OH \quad \text{(R15)}$$

$$C_2H_2 + HO_2 \rightleftarrows CH_2O + HCO \quad \text{(R16)}$$

$$C_2H_2 + HO_2 \rightleftarrows CH_3O + CO \quad \text{(R18)}$$

$$C_2H_2 + HO_2 \rightleftarrows CH_3 + CO_2 \quad \text{(R19)}$$

$$C_2H_2 + HO_2 \rightleftarrows CH_2CHOO \quad \text{(R20)}$$

The temperature and pressure dependent rate coefficients for these eight reactions were adopted from the recent analysis of the C_2H_3 + O_2 kinetics by Goldsmith et al. [43].

HO_2 can add directly to the triple bond in C_2H_2 to form hydroperoxyl-vinyl, CHCHOOH, shown in black, or it can undergo a concerted pathway in which the O-H bond is broken during the O-addition to form vinyl-peroxy, CH_2CHOO, shown in yellow. CHCHOOH easily cleaves the O-O bond to form OH + triplet CHCHO. CH_2CHOO can undergo several reactions, the three most significant of which are: (i) C-O bond cleavage to form C_2H_3 + O_2 (shown in orange), (ii) O-O bond cleavage to form CH_2CHO + O (shown in blue), or (iii) isomerization to dioxiranyl-methyl, c-$CH(CH_2)OO$, which isomerizes to oxyranyloxy, c-$CH(O)CH_2O$, thereby breaking the O-O bond (shown in red). From c-$CH(O)CH_2O$, numerous highly exothermic pathways are available, the most significant of which is CH_2O + HCO.

The stationary points in Fig. 1 were computed using a combination of electronic structure methods. Most stationary points were computed using a post-coupled cluster compound method, which is expected to be accurate to $\pm$0.3 kcal/mol at two standard deviations. Several of the key transition states required multi-reference calculations. For complete details of the methods, the reader is referred to Ref. [43].

In the context of C_2H_2 + HO_2, the most important transition states are (i) O-O bond fission in CHCHOOH, (ii) C-O bond-fission in CH_2CHOO, and

(iii) O-O bond-fission in CH_2CHOO. Notably, all three of these transition states required multi-reference calculations. For $CHCHOOH \rightarrow {}^3CHCHO + OH$, the active space included the 2 π, π^* orbitals and the radical orbital in ^3CHCHO, plus the radical orbital in OH; these calculations were averaged over two states to account for the orbital degeneracy of the OH radical. For $CH_2CHOO \rightarrow C_2H_3 + O_2$, the active space included the 4 π, π^* orbitals in O_2, the 2 π, π^* orbitals in C_2H_3, and the carbon radical. For $CH_2CHOO \rightarrow CH_2CHO + O$, the active space included the 2 π, π^* orbitals and the radical orbital in CH_2CHO, plus the 3 2p orbitals of the O atom; these calculations were averaged over three states to account for the three-fold degeneracy at infinite separation.

For $CHCHOOH \rightarrow {}^3CHCHO + OH$ and $CH_2CHOO \rightarrow C_2H_3 + O_2$, Variable Reaction Coordinate Transition State Theory was used to determine the location of the transition state dividing surface [44, 45]. In VRC-TST, the internal degrees of freedom for the evaluation of the partition function are separated into conserved and transitional modes. The conserved modes are the normal modes of the two fragments at infinite separation, and the transitional modes, are the coupled, anharmonic relative motion of the two fragments. The configuration integral is evaluated using Monte Carlo integration. The transition state for $CH_2CHOO \rightarrow CH_2CHO + O$, in contrast, has a more pronounced saddle point; variational transition state theory was used to determine the minimum flux for the O-O bond distance of 1.70 to 2.05 Ångstroms.

The temperature- and pressure-dependent phenomenological rate coefficients were computed using the RRKM/ME code, which was recently developed at Argonne National Laboratory [46, 47]. Collisional energy transfer was

represented by a single exponential down model, given by 200 $(T/300)^{0.85}$ cm^{-1}. A Lennard-Jones (LJ) collision model was used to determine the collision frequency. The LJ parameters for the bath gas were $\sigma_{He} = 2.55$ Å and $\epsilon_{He} = 6.96$ cm^{-1}, and the LJ parameters for the $C_2H_3O_2$ intermediates were $\sigma_{C_2H_3O_2} = 5.18$ Å and $\epsilon_{C_2H_3O_2} = 285.2$ cm^{-1}. For additional details of the RRKM/ME calculations, see Ref. [43].

Reaction of C_2H_2 with O_2

The initiation involving acetylene and oxygen may proceed as a direct reaction,

$$C_2H_2 + O_2 \longrightarrow \text{products}$$

or through isomerization to vinylidene, followed by reaction of this radical with O_2,

$$C_2H_2(+M) \rightleftarrows H_2CC(+M) \qquad \text{(R1)}$$

$$H_2CC + O_2 \rightleftarrows CH_2 + CO_2 \qquad \text{(R22)}$$

In a number of modeling studies [5, 6, 8, 11, 12, 48–50], the direct reaction of C_2H_2 with O_2 (R15) was proposed to be important for initiation. The reaction has several possible product channels, but predictions are mainly sensitive to the overall rate constant, provided that radicals are formed. There are no measurements of the reaction rate and the rate constant is quite uncertain with calculated barriers ranging from 30 [51] to 51-66 kcal mol^{-1} [50, 52].

In the present work, the potential energy surface for oxygen interacting with acetylene has been explored computationally. Geometries of stationary points were located via QCISD theory with the 6-311G(d,p) basis set, using the Gaussian 09 program [53], and verified to be minima or transition states

via their vibrational frequencies. For the purpose of estimating zero-point vibrational energy these frequencies were scaled by 0.978 [54]. Single-point energies were obtained by extrapolation of CCSD(T) energies to the complete basis set (CBS) limit with the aug-cc-pVTZ and aug-cc-pVQZ basis sets, and corrected for core-valence, relativistic and zero-point effects. The Molpro 2010 program was used here [55]. Details are summarized in the Supplementary Information. As a check on the reliability of the relative enthalpies we derive, we note that computed reaction enthalpy to make glyoxal at 0 K of -104.7 kcal mol^{-1} is 0.6 kcal mol^{-1} too negative compared to the experimental value of -104.1 $\pm$ 0.14 kcal mol^{-1} [56]. A rough estimate of the uncertainty in these calculations is therefore of the order of 1 kcal mol^{-1}.

Figure 3 shows that oxygen can add to acetylene over a significant barrier to form a metastable triplet adduct with one C-O bond. This peroxy biradical can isomerize to singlet oxyethylene, that has a four-membered ring, which then opens via O-O cleavage to yield glyoxal. This is formed with an energy far in excess of that needed to dissociate via molecular and radical channels. Given that HCO + HCO formation is favored by high temperature and high bath gas density for thermal decomposition [57], HCO seems a plausible product in this chemically activated system. This HCO will of course rapidly dissociate to H + CO at elevated temperatures, especially as it may be formed vibrationally hot. The bottleneck to this process is isomerization of the initial triplet adduct, which requires intersystem crossing (ISC) to the singlet PES. We have searched for the minimum energy crossing point in this region using a locally modified version of Harvey's MECP program [58]. Figure 4 shows the structure obtained at the CCSD/aug-cc-pVTZ level of theory, where ring closure by formation of a second C-O bond can be seen. CCSD/6-311G(d,p) vibrational frequencies were obtained at the corresponding geometry. This

level of theory was applied to the triplet adduct as well, and the relative enthalpy of the MECP is 12.5 kcal mol^{-1}. Combined with data for the adduct, this yields an enthalpy for the MECP of 48.6 kcal mol^{-1} relative to the reactants at 0 K.

Because there is a small barrier to exothermic dissociation of the triplet adduct back to the reactants, we can imagine that a small population is maintained in equilibrium with $C_2H_2 + O_2$. The O-O-C bending mode moves the adduct towards the MECP, and because there is a bound adduct the system may explore the MECP multiple times during the short lifetime of the triplet adduct. Thus, even though the probability of ISC may be small for a single encounter at the MECP, we will treat the overall rate of reaction as though this probability is effectively 1. Similar arguments have been made for spin-forbidden chemistry arising from $C_2H_2 + O(^3P)$ atoms [59]. For an upper limit to the reactivity, here we treat the MECP analogously to a simple transition state, which yields $k_{C_2H_2+O_2}$ = 6.08 x 10^{12} exp(-26800 K/T) cm^3 mol^{-1} s^{-1}.

Figure 5 shows an Arrhenius plot for the $C_2H_2 + O_2$ reaction, comparing the present rate constant with (theoretical) values from the literature. Benson [51] proposed a low barrier (30 kcal mol^{-1}) pathway to formyl radicals; Miller and coworkers [42] adopted this value and estimated a pre-exponential factor. Sheng and Bozzelli [52] made an ab initio molecular orbital and density functional analysis of the reaction proceeding along the triplet surface. They found the overall rate constant at atmospheric pressure to be k = $2.2 \cdot 10^7$ $T^{1.41}$ exp(-16600/T) cm^3 mol^{-1} s^{-1}, with HCO + HCO being the major product channel and formation of OCHCHO constituting about 10%. As seen in Fig. 5, the present value of k_{21} is several orders of magnitude lower

than the rate constants from these previous studies.

Laskin and Wang [50] concluded that the direct attack of O_2 on the π bond in acetylene had a larger energy barrier than acetylene $\rightleftarrows$ vinylidene isomerization, so that the sequence

$$C_2H_2(+M) \rightleftarrows H_2CC(+M) \tag{R1}$$

$$H_2CC + O_2 \rightleftarrows CH_2 + CO_2 \tag{R22}$$

would be energetically favorable compared to the direct reaction. They proposed a rate constant for the sequence (R1), (R22), based on the assumption of partial equilibration of (R1). This rate constant, which is also included in Fig. 5, is indeed larger than our calculated value of k_{21}, supporting the idea that the vinylidene sequence is more important for initiation than (R21).

Detailed Kinetic Model

The starting mechanism and corresponding thermodynamic properties were drawn from previous mechanisms for high-pressure oxidation of small hydrocarbons [34–39]. The thermodynamic properties for selected species are shown in Table 1, while Table 2 lists key reactions in the C_2H_2 oxidation scheme. In the following, the numbering of the reactions corresponds to the numbers in this table. The full mechanism is available as supplemental material.

A special feature of the mechanism is that it takes into account the prompt dissociation of the weakly bound radical HCO, based on the recent work of Labbe et al. [67]. Weakly bound free radicals have low dissociation thresholds, facilitating dissociation during the vibrational-rotational relaxation pro-

cess at high temperatures where the timescales for dissociation and collisional relaxation become comparable. The prompt dissociation of HCO yields atomic hydrogen, promoting the radical pool. We adopt the results of the dynamics calculations of Labbe et al. for OH + CH_2O and H + CH_2O, while for other HCO-forming reactions, an approximate method was used to derive prompt dissociation fractions [67]. This modification of the mechanism is not important for the high pressure, intermediate temperature conditions of the present experimental work, but has an impact on flame speed calculations.

Little work has been reported on the low-to-medium temperature oxidation chemistry for acetylene, neither at atmospheric nor at higher pressures. The early static reactor work [1, 2], covering the temperature range 463-673 K, was entirely experimental. More recent reactor studies of Tan et al. [5] and Alzueta et al. [6], conducted at temperatures of 800–1100 K and 700-1500 K, respectively, involved kinetic modeling, but at pressures significantly below those of the present study. To account for the high pressure, we have updated the C_2H_2 oxidation subset of the mechanism, with particular emphasis on the initiation chemistry.

As discussed above, the reaction $C_2H_2 + O_2 \rightarrow$ products and the sequence $C_2H_2(+M) \rightleftarrows H_2CC(+M)$ (R1), $H_2CC + O_2 \rightarrow$ products have been proposed as initiation steps for acetylene oxidation. The rate constant for the isomerization step (R1) was evaluated by Laskin and Wang [50], but only at the low pressure limit. The high-pressure rate constant is not well established, but under most practical conditions (R1) is rapidly equilibrated. The subsequent reaction of vinylidene with O_2 was assumed to be fast, forming CH_2 + CO_2 (R22).

Upon initiation, the key consumption step for acetylene is the reaction with

OH (R7). This reaction, which is also important for consumption of C_2H_2 in the atmosphere, has been characterized experimentally and theoretically over a wide range of conditions [60, 66, 68–71]. Recent theoretical studies [66, 71] identify five important channels, i.e. CHCHOH (R7), CH_3+CO (R8), HCCOH+H (R9), CH_2CO+H (R10), and C_2H+H_2O (R11). The relative importance of the five channels is a complex function of pressure and temperature. Under the conditions of the present work, with high pressure and temperatures of 600–900 K, the recombination reaction to form the adduct (R7) is the dominant channel for C_2H_2+OH. We have adopted the rate coefficients of Senosaian et al. [66], which agree well with reported experimental data.

Other consumption steps of acetylene include reaction with H, O, and HO_2. The H-abstraction reaction (R3b) has a significant barrier and it is quite slow, so C_2H_2 + H largely leads to formation of vinyl (R2) under the present conditions, augmented by the high pressure. Vinyl reacts mostly with O_2 under stoichiometric and oxidizing conditions. This step is a complex multi-well, multi-channel process occurring on the same PES as C_2H_2 + HO_2. As discussed above, the reaction was studied recently by Goldsmith et al. [43], based on state-of-the-art calculations of the $C_2H_3O_2$ potential energy surface. Here, their recommendation was preferred to earlier theoretical studies of this reaction [38, 72–74]. For C_2H_2 + O, we use the rate constants for the two major channels, HCCO + H (R4) and CH_2 + CO (R5) proposed by Miller and coworkers [42]; these values represent well available experimental results.

The C_2H_2 + HO_2 reaction yields triplet formylmethylene (^{3}CHCHO) as a major product (R12). A subset for the ^{3}CHCHO radical was included in the mechanism with estimated rate constants. The ^{3}CHCHO radical is a triplet carbene like triplet methylene ($^3CH_2$) and rate constants were assumed to

be similar. Similarly to the methylene radical, the triplet ground state and the lowest singlet state for formylmethylene are separated only by a small difference in energy; computations show a 2 kcal mol^{-1} energy for the singlet state above the triplet ground state [75]. Here we have included reactions only for the triplet state; in future work both the triplet and singlet states of the radical should be taken into account.

The CHCHOH adduct, formed by (R7), may decompose thermally, react with the O/H radical pool, or with stable species such as O_2. However, the fast reaction with O_2 is the major consumption step, even at higher temperatures. Alzueta et al. [6] identified the chain-propagating sequence

$$C_2H_2 \xrightarrow{+OH} C_2H_2OH \xrightarrow{+O_2} OCHCHO + OH$$

as important for the onset of reaction for C_2H_2 at atmospheric pressure and temperatures above 700 K. Interest in this oxidation pathway for atmospheric chemistry has spawned a range of experimental and theoretical studies on the C_2H_2 + OH + O_2 reaction at low temperature [41, 76–85]. Hatakeyama et al. [76] showed in smoke-chamber experiments that the reaction generates glyoxal and formic acid,

$$CHCHOH + O_2 \rightleftarrows OCHCHO + OH \tag{R23}$$

$$CHCHOH + O_2 \rightleftarrows HOCHO + HCO \tag{R24}$$

Unlike the CH_2CH_2OH+O_2 reaction, which forms $HOCH_2CH_2OO$ at high pressure and low temperature [38], stabilization of the HOCHCHOO radical is negligible. Hatakeyama et al. showed that the product yields of the reaction were unaffected by addition of NO, known to react rapidly with peroxides. This demonstrates that the formation of products occurs directly from the peroxy radical. The finding that HOCHCHOO is shortlived and

leads to regeneration of the OH radical has been confirmed in a number of experimental and theoretical studies [41, 77–85].

Reported data on the branching fraction at low temperature are in good agreement. Hatakeyama et al. reported the yield of glyoxal to be 0.7±0.3 and that of formic acid to be 0.4±0.1. Bohn et al. [41, 78, 79] confirmed the yield of 0.7 for glyoxal + OH from flash photolysis studies, while the theoretical work by Maranzana et al. [81, 82] indicates a branching fraction of 53%. In a recent study, Glowacki et al. [85] determined the branching fraction experimentally for 200-450 K. Their experimental data can crudely be fit to the form α = 0.55 exp(94/T) exp(-0.3 X_{O_2}) where α is the yield of OH from CHCHOH + O_2 and X_{O_2} is the mole fraction of O_2.

The only measurement of the rate constant for the CHCHOH + O_2 reaction [77] indicates a value for the OH regeneration channel (R23) of 2.5 x 10^{12} cm^3 mol^{-1} s^{-1} at 0.26 atm. We have combined this value with the expression for the branching fraction from Glowacki et al. [85] to obtain the rate constants for (R23) and (R24). The results of Glowacki et al. are independent of the total pressure over 10-75 torr, and that might be expected to hold at higher pressures because the branching ratio depends mainly on competition between reaction with O_2 and collisional quenching.

Since glyoxal and formic acid are important intermediates in acetylene oxidation under the present conditions, the reaction subsets for these species become important. Both subsets were drawn from recent work by the authors; for glyoxal oxidation from Fassheber et al. [61] and for formic acid from Marshall and Glarborg [62]. Experimental data for validation of oxidation mechanisms for glyoxal and formic acid are very limited, and more work on these subset are desirable.

Results and Discussion

Mixtures of C_2H_2 (about 1000 ppm) and O_2 highly diluted in N_2 were reacted at pressures of 50-60 bar and stoichiometries ranging from reducing to oxidizing conditions. The flow rate of 3 L min^{-1} (STP) resulted in (temperature dependent) residence times of 10-15 s in the isothermal zone of the reactor. The diluted conditions ensured a low heat release during the reaction. The experimental data were obtained as mole fractions as a function of the reactor temperature from 600–900 K using intervals of 25 K. The lower bound of the temperature interval (600 K) was well below the temperature for onset of reaction.

Figure 6 compares experimental and modeling results at reducing conditions (excess air ratio $\lambda = 0.18$), whereas data sets obtained at stoichiometric ($\lambda = 0.99$) and oxidizing ($\lambda = 19.4$) conditions are presented in Figs. 7 and 8, respectively. The numerical predictions of the concentration profiles were obtained from isothermal calculations using CHEMKIN PRO [86].

The temperature for onset of reaction was approximately 725 K, independent of stoichiometry. Under stoichiometric and oxidizing conditions (Figs. 7 and 8), CO was the only intermediate measured in major concentrations, but it should be noted that species such as CH_2O, HOCHO, and OCHCHO could not be detected due to limitations in the analysis equipment. For stoichiometric conditions, the concentrations of CO, CO_2, and O_2 levelled out above 800 K with CO as the major product, while for lean conditions CO was mostly oxidized to CO_2 at higher temperatures. Under reducing conditions (Fig. 6), CO was the main product, but also formation of C_2H_4 was observed, together with small amounts of CH_4 and C_2H_6.

The modeling predictions are generally in satisfactory agreement with the experimental results. Under reducing conditions (Fig. 6), the onset temperature is predicted accurately, but the model calculates a lower consumption of C_2H_2 at temperatures above 750 K than observed. The levels of CO, CO_2, and CH_4 are predicted well, while the formation of C_2H_4 is overpredicted by a factor of two.

Also under stoichiometric and oxidizing conditions (Figs. 7 and 8), the temperatures for onset of reaction are predicted well. Most species profiles are captured quantitatively, even though at oxidizing conditions, conversion of CO to CO_2 is underpredicted at higher temperatures.

Figure 9 shows the results of a sensitivity analysis for the stoichiometric conditions (Fig. 7). The predicted temperature for onset of reaction is particularly sensitive to steps involving C_2H_2 and to the branching fractions for the reactions of O_2 with C_2H_3 (mostly under reducing conditions) and CHCHOH. The reactions of C_2H_2 with H (R2) and HO_2 (R12), as well as $C_2H_3 + O_2 \rightarrow CH_2CHO + O$ and $CHCHOH + O_2 \rightarrow$ products (R23, R24) enhance reaction, while $C_2H_3 + O_2 \rightarrow CH_2O + HCO/H{+}CO$ inhibits oxidation. In the H_2/O_2 subset, modeling is most sensitive to formation and consumption of HO_2 and H_2O_2.

Figure 10 provides an overview of the major oxidation pathways for C_2H_2, according to the model. The solid lines denote pathways important across stoichiometries while the dashed lines denote pathways important mostly under reducing conditions. Upon initiation, the oxidation pathway depends on the composition of the O/H radical pool. Under stoichiometric and lean conditions, C_2H_2 mainly recombines with OH to form CHCHOH (R7). The CHCHOH adduct then reacts with O_2 to form glyoxal (R23) and formic acid

(R24). Both of these intermediates build up in considerable concentrations; in particular formic acid which according to the model is oxidized only slowly under these conditions. The sequence (R7), (R23), (R24) corresponds to the mechanism reported for oxidation of acetylene under atmospheric conditions [76].

Under reducing conditions, atomic hydrogen becomes more important as a chain carrier and recombination of C_2H_2 with H to form C_2H_3 (R2) competes with C_2H_2 + OH (R7). Vinyl reacts mainly with O_2 and the products of this reaction have a significant impact on the oxidation pathways.

Formation routes for the minor products C_2H_4 and C_2H_6 are not shown. Ethylene, which is overpredicted by the model, is formed from the vinyl radical through H-abstraction reactions with HO_2 and CH_2O. The C_2H_3 + HO_2 reaction forms CH_2CHO + OH as well as C_2H_4 + O_2, and both the rate constant and the branching fraction are uncertain; we use a rate constant for C_2H_4 + O_2 obtained from theory by Hua et al. [87]. The rate constant for C_2H_3 + $CH_2O \rightarrow C_2H_4$ + HCO was drawn from the recent theoretical work of Zador and Miller [88] who studied reactions on the C_3H_5O potential energy surface. Ethane is only formed in small quantities, mainly through the sequence $C_2H_2 \xrightarrow{+O} CH_2 \xrightarrow{+H} CH_3 \xrightarrow{+CH_3} C_2H_6$.

The present work is not intended to be a comprehensive study of acetylene oxidation, but the reviewers of the paper encouraged us to include comparisons of modeling predictions with selected experimental results from literature. Figure 11 presents ignition delay times of $C_2H_2/O_2/Ar$ measured by Eiteneer and Frenklach [13] at an average pressure of 1.2 atm and temperatures between 1150 and 2080 K. For the majority of the mixtures, the model underestimates ignition delays. The same trend is seen in Fig. 12, which

presents ignition delay times of $C_2H_2/O_2/Ar$ measured by Tereza et al. [14] at 6.5 bar. Both sets of experiments show that ignition delays are shorter under fuel-rich conditions, compared to stoichiometric and fuel-lean conditions. The model captures this trend, as well as the sensitivity of ignition delays to temperature.

A brute-force method was used to investigate the sensitivity of reaction rates in predicting ignition delay at low temperatures. As shown in Fig. 13, formation of the vinyl radical and the different branches of the $C_2H_3 + O_2$ reaction controls the ignition delay of C_2H_2 to a large extent. Also reaction of C_2H_2 with OH (R10) and HO_2 (R12) are important for ignition, while formation of CHCHOH is less important.

Figure 14 compares measured flame speeds of C_2H_2/air at atmospheric pressure with modeling results. It is notable that under reducing conditions, the flame speeds reported by Rokni et al. [29] and Egolfopoulos et al. [24] are considerably higher (up to 60%) than those reported by Jomaas et al. [30] and Ravi et al. [31]. The modeling predictions agree well with the lower values [30,31].

Sensitivity of the reactions rates in predicting flame speed is studied via a built-in function in CHEMKIN. As shown in figure 15, the calculated flame speed is highly sensitive to reactions involving H atom. Notably, the competition between $CH_2O+H=H+CO+H_2$ and $CH_2O+H=HCO+H_2$ influences the flame speed calculation considerably. Inclusion of prompt dissociation of HCO [67] in the mechanism serves to increase the predicted flame speeds by several cm/s, enhancing the agreement with experiment.

Figure 16 shows the flame speed of a lean mixture of C_2H_2/O_2 diluted in

N_2/He versus pressure. While the model agrees very well with the atmospheric measurements, it overestimates the flame speed at higher pressures.

Conclusions

A detailed chemical kinetic model for oxidation of acetylene at intermediate temperatures and high pressure has been developed and evaluated experimentally. The rate constants for the reactions of C_2H_2 with HO_2 and O_2 were calculated theoretically. Experiments were conducted with C_2H_2/O_2 mixtures highly diluted in N_2 in a high pressure flow reactor at 600–900 K and 60 bar over a wide range of stoichiometry. Model predictions were generally in satisfactory agreement with the experimental data. Acetylene is mostly consumed by recombination with H to form vinyl (reducing conditions) or with OH to form a CHCHOH adduct (stoichiometric to lean conditions). Both C_2H_3 and CHCHOH then react primarily with O_2. The CHCHOH + O_2 reaction leads to formation of significant amounts of glyoxal (OCHCHO) and formic acid (HOCHO), and the oxidation chemistry of these intermediates is important for the overall reaction.

Acknowledgments

The work is part of the CHEC (Combustion and Harmful Emission Control) research program. It was financially supported by the Technical University of Denmark and the Danish Technical Research Council. JGL would like to thank Ministerio de Ciencia e Innovacion (MICINN) through project CTQ2006-09963 for financial support. PM thanks the R.A. Welch Founda-

tion (Grant B-1174) for support. CFG gratefully acknowledges support from Brown University. Finally, the authors would like to thank the reviewer who identified an error in the Chemkin input file that affected modeling predictions.

References

[1] Hay, J.M.; Norrish, R.G.W. Proc Roy Soc Ser A 1965, 288, 17-38.

[2] Stevenson, T.M.; Tipper, C.F.H. Combust Flame 1967, 11, 35-48.

[3] Hay, J.M.; Lyon, D. Proc Roy Soc Ser A 1970, 317, 1-20.

[4] Williams, A.; Smith, D.B. Chem Revs 1970, 70, 267-293.

[5] Tan, Y.W.; Dagaut, P.; Cathonnet, M.; Boettner, J.C. Combust Sci Technol 1994, 102, 21-55.

[6] Alzueta, M.U.; Borruey, M.; Callejas, A.; Millera, A.; Bilbao, R. Combust Flame 2008, 152, 377-386.

[7] Stubbeman, R.F. J Phys Chem 1964, 68, 3169-3176.

[8] Jachimowski, C.J. Combust Flame 1977, 29, 55-66.

[9] Hidaka, Y.; Eubank, C.S.; Gardiner Jr.; Hwang, S.M. J Phys Chem 1984, 88, 1006-1012.

[10] Hwang, S.M.; Gardiner Jr.; W.C.; Frenklach, M.; Hidaka, Y. Combust Flame 1987, 67, 65-75.

[11] Hidaka, Y.; Hattori, K.; Okuno, T.; Inami, K.; Abe, T.; Koike, T. Combust Flame 1996, 107, 401-417.

[12] Ryu, J.C.; Seo, H.; Kang, J.G.; Oh, K.H. Bull Korean Chem Soc 1996, 18, 1071-1075.

[13] Eiteneer, B.; Frenklach, M. Int J Chem Kinet 2003, 35, 391-414.

[14] Tereza, A.M.; Slutskii, V.G.; Severin, E.S. Russ J Phys Chem B 2009, 3, 99-108.

[15] Gibbs, G.J.; Calcote, H.F. J Chem Engn Data 1959, 4, 226-237.

[16] Scholte, T.G.; Vaags, P.B. Combust Flame 1959, 3, 495-501.

[17] Bonne, U.; Homann, K.H.; Wagner, H.Gg. Proc Combust Inst 1964, 10, 503-512.

[18] Eberius, K.H.; Hoyermann, K.; Wagner, H.Cg. Proc Combust Inst 1973, 14, 147-156.

[19] Vandooren, J.; Van Tiggelen, P.J. Proc Combust Inst 1976, 16, 1133-1144.

[20] Warnatz, J.; Bockhorn, H.; Moser, A.; Wenz, H. Proc Combust Inst 1982, 19, 197-209.

[21] Westmoreland, P.R.; Howard, J.B.; Longwell, J.P. Proc Combust Inst 1986, 21, 773-782.

[22] Bastin, E.; Delfau, J.-L.; Reuillon, M.; Vovelle, C.; Warnatz, J. Proc Combust Inst 1988, 22, 313-322.

[23] Miller, J.A.; Volponi, J.V.; Durant, J.L.; Goldsmith, J.E.M.; Fisk, G.A.; Kee, R.J. Proc Combust Inst 1990, 23, 187-194.

[24] Egolfopoulos, F.N.; Zhu, D.L.; Law, C.K. Proc Combust Inst 1990, 23, 471-478.

[25] Doute, C.; Delfau, J.-L.; Vovelle, C. Combust Sci Technol 1994, 103, 153-173.

[26] Lamprecht, A.; Atakan, B.; Kohse-Hoinghaus, K. Combust Flame 2000, 122, 483-491.

[27] Ancia, R.; Van Tiggelen, P.J.; Vandooren, J. Exp Thermal Fluid Sci 2004, 28, 715-722.

[28] Li, Y.Y.; Zhang, L.D.; Tian, Z.Y.; Yuan, T.; Zhang, K.W.; Yang, B.; Qi, F. Proc Combust Inst 2009, 32, 1293-1300.

[29] Rokni, E.; Moghaddas, A.; Askari, O.; Metghalchi, H. J Energy Resour Technol 2015, 137, 012204.

[30] Jomaas, G.; Zheng, X.L.; Zhu, D.L.; Law, C.K. Proc Combust Inst 2005, 30, 193-200.

[31] Ravi, S.; Sikes, T.G; Morones, A.; Keesee, C.L.; Petersen, E.L. Proc Combust Inst 2015, 35, 679-686.

[32] Shen, X.; Yang, X.; Santner, J.; Sun, J.; Ju, Y. Proc Combust Inst 2015, 35, 721-728.

[33] Lindstedt, R.P.; Skevis, G. Combust Sci Technol 1997, 125, 73-137.

[34] Hashemi, H.; Christensen, J.M.; Gersen, S.; Glarborg, P. Proc Combust Inst 2015, 35, 553-560.

[35] Rasmussen, C.L.; Hansen, J.; Marshall, P.; Glarborg, P. Int J Chem Kinet 2008, 40, 454-480.

[36] Rasmussen, C.L.; Jacobsen, J.G.; Glarborg, P. Int J Chem Kinet 2008, 40, 778-807.

[37] Hashemi, H.; Christensen, J.M.; Gersen, S.; Levinsky, H.; Klippenstein, S.J.; Glarborg, P. "High-Pressure Oxidation of Natural Gas: Methane", submitted for publication (2016).

[38] Gimenez-Lopez, J.; Rasmussen, C.L.; Alzueta, M.U.; Marshall, P.; Glarborg, P. Proc Combust Inst 2009, 32, 367-375.

[39] Gimenez, J.; Alzueta, M.U.; Rasmussen, C.L.; Marshall, P., Glarborg, P. Proc Combust Inst 2011, 33, 449-457.

[40] Aranda, V.; Christensen, J.M.; Alzueta, M.U.; Glarborg, P.; Gersen, S.; Gao, Y.; Marshall, P. Int J Chem Kinet 2013, 45, 283-294.

[41] Bohn, B.; Zetzsch, C. J Chem Soc, Faraday Trans 1998, 94, 1203-1210.

[42] Glarborg, P.; Alzueta, M.U.; Dam-Johansen. K.; Miller, J.A. Combust Flame 1998, 115, 1-27.

[43] Goldsmith, C.F.; Harding, L.B.; Georgievskii, Y.; Miller, J.A.; Klippenstein, S.J. J Phys Chem A 2015, 119, 7766-7779.

[44] Klippenstein, S.J. J Chem Phys 1992, 96, 367-371.

[45] Georgievskii, Y.; Klippenstein, S.J. J Phys Chem A 2003, 107, 9776-9781.

[46] Georgievskii, Y.; Miller, J.A.; Burke, M.P.; Klippenstein, S.J. J Phys Chem A 2013, 117, 12146-12154.

[47] Georgievskii, Y.; Jasper, A.W.; Zador, J.; Miller, J.A.; Burke, M.P.; Goldsmith, C.F.; Klippenstein, S.J. "PAPER: Predictive Automated Phenomenological Elementary Rates", version 1.0, Argonne National Laboratory.

[48] Miller, J.A.; Mitchell, R.E.; Smooke, M.D.; Kee, R.J. Proc Combust Inst 1982, 19, 181.

[49] Skjøth-Rasmussen, M.S.; Glarborg, P.; Østberg, M.; Larsen, M.B.; Sørensen, S.W.; Johnsson, J.E.; Jensen, A.D.; Christensen, T.S. Proc Combust Inst 2002, 29, 1329-1336.

[50] Laskin, A.; Wang, H. Chem Phys Lett 1999, 303, 43-49.

[51] Benson, S.W. Int J Chem Kinet 1996, 28, 665-672.

[52] Sheng, C.; Bozzelli, J.W. Int J Chem Kinet 2000, 32, 623-641.

[53] Frisch, M. J.; et al. Gaussian 09; Gaussian: Wallingford, CT, 2010.

[54] Johnson, III, R.D. NIST Computational Chemistry Comparison and Benchmark Database, in: NIST Standard Reference Database Number 101, 2013.

[55] MOLPRO, version 2010.1, a package of ab initio programs, in, Werner et al. MOLPRO, version 2010.1, a package of ab initio programs, 2010.

[56] B. Ruscic. Active Thermochemical Tables (ATcT) values based on ver. 1.112 of the Thermochemical Network (2013); available at ATcT.anl.gov.

[57] Friedrichs, G.; Colberg, M.; Dammeier, J.; Bentz, T.; Olzmann, M. Phys Chem Chem Phys 2008, 10, 6520-6533.

[58] Harvey, J.N. Geometry Optimization of an MECP, see http://www.chm.bris.ac.uk/pt/harvey/spinforbidden.htm, 2003.

[59] Rajak, K.; Maiti, B. J Chem Phys 2010, 133, 011101.

[60] Fulle, D.; Hamann, H.F.; Hippler, H.; Jansch, C.P. Ber Bunsenges Phys Chem 1997, 101, 1433-1442

[61] Fassheber, N.; Friedrichs, G.; Marshall, P.; Glarborg, P. J Phys Chem A 2015, 119, 7305-7315.

[62] Marshall, P. Glarborg, P. Proc Combust Inst 2015, 35, 153-160.

[63] Miller, J.A.; Klippenstein, S.J. Phys Chem Chem Phys 2004, 6, 1192-1202.

[64] Harding, L.B.; Schatz, G.C.; Chiles, R.A. J Chem Phys 1982, 76, 5172-5173.

[65] Glarborg, P.; Miller, J.A.; Kee, R.J. Combust Flame 1986, 65, 177-202.

[66] Senosiain, J.P.; Klippenstein, S.J.; Miller, J.A. J Phys Chem A 2005, 109, 6045-6055.

[67] Labbe, N.J.; Sivaramakrishnan, R.; Goldsmith, C.F.; Georgievski, Y.; Miller, J.A.; Klippenstein, S.J. J Phys Chem Lett 2016, 7, 85-89.

[68] Smith, G.P.; Fairchild, P.W.; Crosley, D.R. J Chem Phys 1984, 81, 2667-2677.

[69] Srinivasan, N.K.; Su, M.-C.; Michael, J.V. Phys Chem Chem Phys 2007, 9, 4155-4163.

[70] Sørensen, M.; Kaiser, E.W.; Hurley, M.D.; Wallington, T.J.; Nielsen, O.J. Int J Chem Kinet 2003, 35, 191-197.

[71] McKee, K.W.; Blitz, M.A.; Cleary, P.A.; Glowacki, D.R.; Pilling, M.J.; Seakins, P.W.; Wang, L.M. J Phys Chem A 2007, 111, 4043-4055

[72] Mebel, A.M.; Diau, E.W.G.; Lin, M.C.; Morokuma, K. J Am Chem Soc 1996, 118, 9759-9771.

[73] Carriere, T.; Westmoreland, P.R.; Kazakov, A.; Stein, Y.S.; Dryer, F.L. Proc Combust Inst 2002, 29, 1257-1266.

[74] Matsugi, A.; Miyoshi, A. Int J Chem Kinet 2014, 46, 260-274.

[75] Guan, J.; Randall, K.R.; SchaeferIII, H.F.; Li, H. J Phys Chem A 2013, 117, 2152-2159

[76] Hatakeyama, S.; Washida, N.; Akimoto, H. J Phys Chem 1986, 90, 173-178.

[77] Siese, M.; Zetzsch, C. Z Phys Chem 1995, 188, 75-89.

[78] Bohn, B.; Siese, M.; Zetzsch, C.J. Chem Soc, Faraday Trans 1996, 92, 1459-1466.

[79] Bohn, B.; Zetzsch, C. Phys Chem Chem Phys 1999, 1, 5097-5107.

[80] Yeung, L.Y.; Pennino, M.J.; Miller, A.M.; Elrod, M.J. J Chem Phys A 2005, 109, 1879-1889.

[81] Maranzana, A.; Ghigo, G.; Tonachini, G.; Barker, J.R. J Chem Phys A 2008, 112, 3656-3665.

[82] Maranzana, A.; Barker, J.R.; Tonachini, G. J Chem Phys A 2008, 112, 3666-3675.

[83] Galano, A.; Ruiz-Suarez, L.G.; Vivier-Bunge, A. Theor Chem Account 2008, 121, 219-225.

[84] Glowacki, D.R.; Pilling, M.J. ChemPhysChem 2010, 11, 3836-3843.

[85] Glowacki, D.R.; Lockhart, J.; Blitz, M.A.; Klippenstein, S.J.; Pilling, M.J.; Robertson, S.H.; Seakins, P.W. Science 2012, 337, 1066-1069.

[86] CHEMKIN-PRO 15131, Reaction Design, 2013.

[87] Hua, H.; Ruscic, B.; Wang, B. Chem Phys 2005, 311, 335-341.

[88] Zador, J.; Miller, J.A. Proc Combust Inst 2015, 35, 181-188.

Species	H_{298}	S_{298}	$C_{p,300}$	$C_{p,400}$	$C_{p,500}$	$C_{p,600}$	$C_{p,800}$	$C_{p,1000}$	$C_{p,1500}$	Ref.
CHCHOH	27.30	62.49	13.88	16.67	18.86	20.57	23.01	24.68	27.34	[60]
^{3}CHCHO	61.76	62.82	13.12	15.21	16.89	18.21	20.00	21.17	22.77	[43]
OCHCHO	-50.69	65.11	14.48	17.06	19.46	21.49	24.24	25.96	28.05	See [61]
OCHCO	-14.13	67.22	13.82	15.57	17.06	18.32	20.23	21.55	23.48	See [61]
HOCHO	-90.47	59.06	9.90	11.50	13.09	14.50	16.57	18.12	20.39	See [62]
HOCO	-44.33	60.07	10.69	12.01	13.12	14.04	15.35	16.27	17.70	See [62]
OCHO	-30.45	61.27	11.65	12.88	13.97	14.89	16.30	17.24	18.52	See [62]

Table 1: Thermodynamic properties of selected species in the reaction mechanism. Units are kcal mol^{-1} for H, and cal mol^{-1} K^{-1} for S and C_p. Temperature (T) range is in K.

		A	β	E_a	Source
1.	$C_2H_2(+M) \rightleftarrows H_2CC(+M)$	1.8E04	3.510	43300	*a*
	Low pressure limit:	2.5E15	–0.640	49700	[50]
	Troe parameters: 0.5 1.E-30 1.E30				
2.	$C_2H_2 + H(+M) \rightleftarrows C_2H_3(+M)$	1.7E10	1.266	2709	[63]
	Low pressure limit:	6.3E31	–4.664	3780	
	Troe parameters: 0.7878 –10212 1.E-30				
3.	$C_2H + H_2 \rightleftarrows C_2H_2 + H$	4.1E05	2.390	864	[64]
4.	$C_2H_2 + O \rightleftarrows HCCO + H$	1.4E07	2.000	1900	[42]
5.	$C_2H_2 + O \rightleftarrows CH_2 + CO$	6.1E06	2.000	1900	[42]
6.	$C_2H_2 + O \rightleftarrows C_2H + OH$	3.2E15	–0.600	15000	[65]
7.	$C_2H_2 + OH \rightleftarrows CHCHOH$	1.5E24	-4.060	3261	[66], 10 atm, *b*, *c*
		4.5E31	-5.920	8761	[66], 10 atm, *b*, *c*
		6.2E20	-2.800	2831	[66], 100 atm, *b*, *c*
		1.6E29	-4.910	9734	[66], 100 atm, *b*, *c*
8.	$C_2H_2 + OH \rightleftarrows CH_3 + CO$	4.3E08	0.920	3736	[66], 10 atm, *b*
		8.3E05	1.770	4697	[66], 100 atm, *b*
9.	$C_2H_2 + OH \rightleftarrows HCCOH + H$	3.2E06	1.970	12810	[66], 10 atm, *b*
		7.4E06	1.890	13603	[66], 100 atm, *b*
10.	$C_2H_2 + OH \rightleftarrows CH_2CO + H$	5.1E06	1.650	3400	[66], 10 atm, *b*
		1.5E04	2.450	4477	[66], 100 atm, *b*
11.	$C_2H_2 + OH \rightleftarrows C_2H + H_2O$	2.6E06	2.140	8586	[66]
12.	$C_2H_2 + HO_2 \rightleftarrows CHCHO + OH$	5.4E10	0.61	20740	see text, 10 atm, *b*, *c*
		1.6E08	1.36	15420	10 atm, *b*, *c*
		1.5E11	0.48	17730	100 atm, *b*, *c*
		7.2E06	1.73	16020	100 atm, *b*, *c*
13.	$C_2H_2 + HO_2 \rightleftarrows CH_2CHO + O$	7.5E14	-1.17	18350	see text, 10 atm, *b*, *c*
		2.9E-01	3.38	10590	10 atm, *b*, *c*
		5.8E18	-2.09	24350	100 atm, *b*, *c*
		1.1E-01	3.52	11980	100 atm, *b*, *c*
14.	$C_2H_2 + HO_2 \rightleftarrows OCHCHO + H$	4.1E16	-2.03	17630	see text, 10 atm, *b*, *c*
		2.0E-02	3.38	8696	10 atm, *b*, *c*
		5.9E21	-3.32	25030	100 atm, *b*, *c*
		6.8E-02	3.27	10760	100 atm, *b*, *c*
15.	$C_2H_2 + HO_2 \rightleftarrows CH_2CO + OH$	4.7E-05	4.22	16780	see text, 10 atm, *b*, *c*
		8.4E-22	8.76	8804	10 atm, *b*, *c*
		3.6E03	1.97	23010	100 atm, *b*, *c*
		6.6E-12	6.15	14730	100 atm, *b*, *c*
16.	$C_2H_2 + HO_2 \rightleftarrows CH_2O + HCO$	7.3E35	-7.77	26970	see text, 10 atm, *b*, *c*
		9.8E06	0.91	11710	10 atm, *b*, *c*
		2.5E16	-1.70	20030	100 atm, *b*, *c*
		4.3E-06	4.31	6829	100 atm, *b*, *c*
17.	$C_2H_2 + HO_2 \rightleftarrows CH_2O + H + CO$	1.7E36	-7.77	26970	see text, 10 atm, *b*, *c*
		2.3E07	0.91	11710	10 atm, *b*, *c*
		5.8E16	-1.70	20030	100 atm, *b*, *c*
		1.0E-05	4.31	6829	100 atm, *b*, *c*
18.	$C_2H_2 + HO_2 \rightleftarrows CH_3O + CO$	3.3E23	-4.45	21210	see text, 10 atm, *b*, *c*
		2.9E02	1.84	10460	10 atm, *b*, *c*
		1.2E18	-2.57	22360	100 atm, *b*, *c*
		6.9E-04	3.42	9329	100 atm, *b*, *c*
19.	$C_2H_2 + HO_2 \rightleftarrows CH_3 + CO_2$	8.6E28	-6.15	24030	see text, 10 atm, *b*, *c*
		1.9E04	1.26	11230	10 atm, *b*, *c*
		1.7E15	-1.80	20370	100 atm, *b*, *c*
		3.9E-07	4.21	7314	100 atm, *b*, *c*

20.	$C_2H_2 + HO_2 \rightleftarrows CH_2CHOO$	4.6E43	-10.24	26930	see text, 10 atm, *b*, *c*
		2.1E21	-3.78	13380	10 atm, *b*, *c*
		2.5E35	-7.26	26390	100 atm, *b*, *c*
		1.4E19	-2.91	13420	100 atm, *b*, *c*
21.	$C_2H_2 + O_2 \rightleftarrows HCO + HCO$	6.1E12	0.000	53250	pw, *b*
22.	$H_2CC + O_2 \rightleftarrows CH_2 + CO_2$	1.0E13	0.000	0	est
23.	$CHCHOH + O_2 \rightleftarrows OCHCHO + OH$	1.8E12	0.000	-187	see text
24.	$CHCHOH + O_2 \rightleftarrows HOCHO + HCO$	3.3E12	0.000	0	see text, *c*
		-1.8E12	0.000	-187	

a: P. Marshall, unpublished results.
b: The resulting rate constant is an interpolation between pressures (PLOG format). Rate coefficients over a wider pressure range are available in Supplemental Material.
c: Duplicate reaction – the resulting rate constant is the sum of the two expressions.

Table 2: Selected reactions from the C_2H_2 hydrocarbon subset. Parameters for use in the modified Arrhenius expression $k = AT^{\beta} \exp(-E/[RT])$. Units are mol, cm, s, cal.

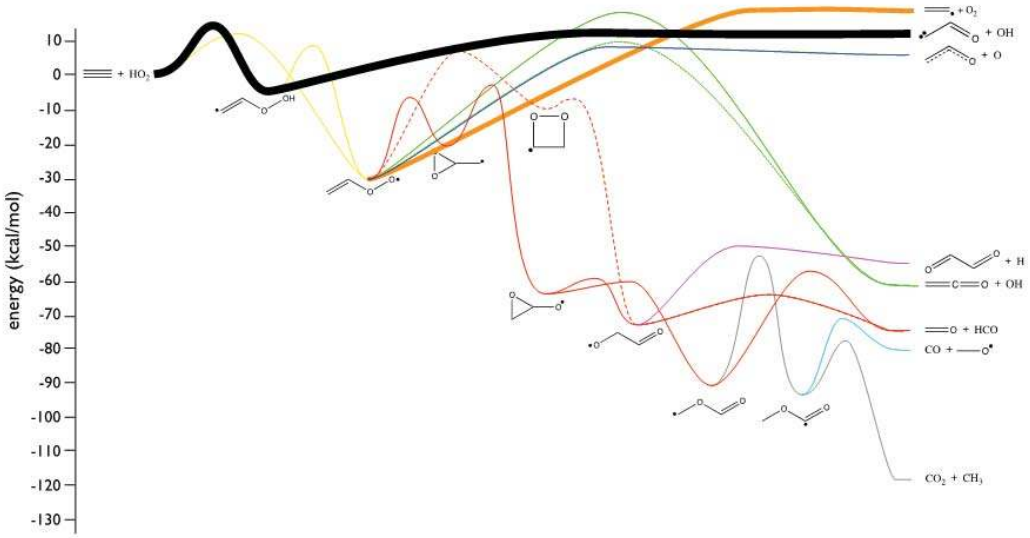

Figure 1: $C_2H_3O_2$ potential energy diagram, relative to C_2H_2 + HO_2. The thick black line is the dominant pathway under the conditions of interest.

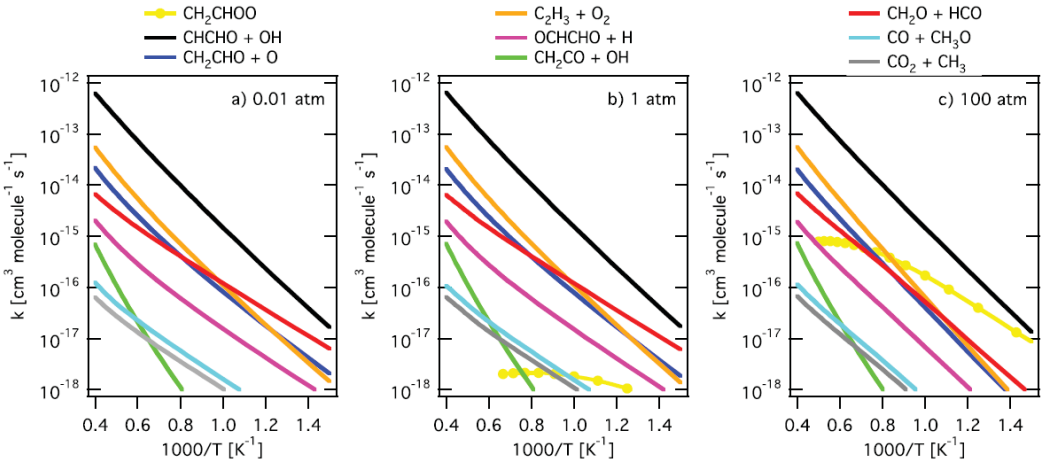

Figure 2: Arrhenius plot for the various product channels formed during $C_2H_2 + HO_2$. The three panels correspond to pressures of (a) 0.01 atm, (b) 1.0 atm, and (c) 100 atm.

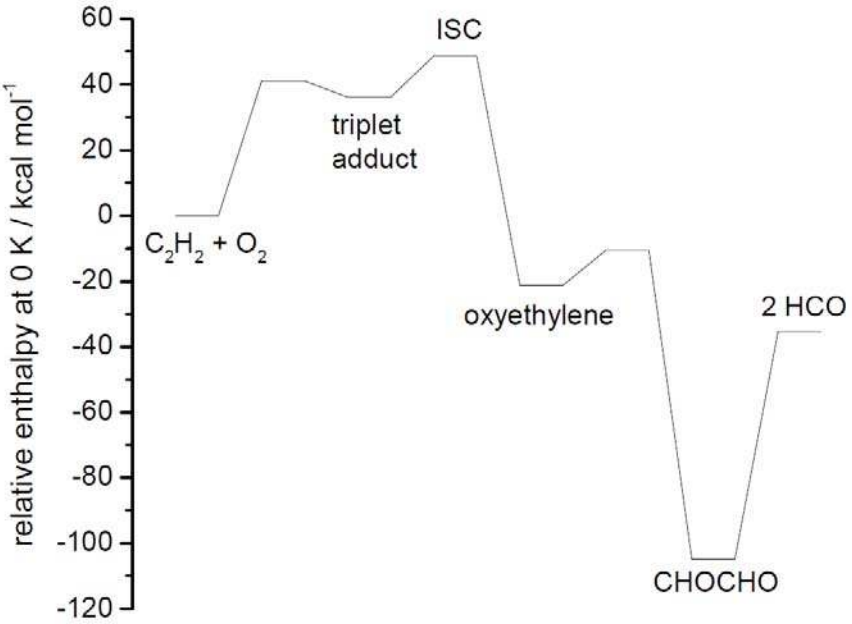

Figure 3: Potential energy diagram for C_2H_2 + O_2 derived via CCSD(T)/CBS theory. See text for details and the methodology for the minimum energy point for intersystem crossing (ISC).

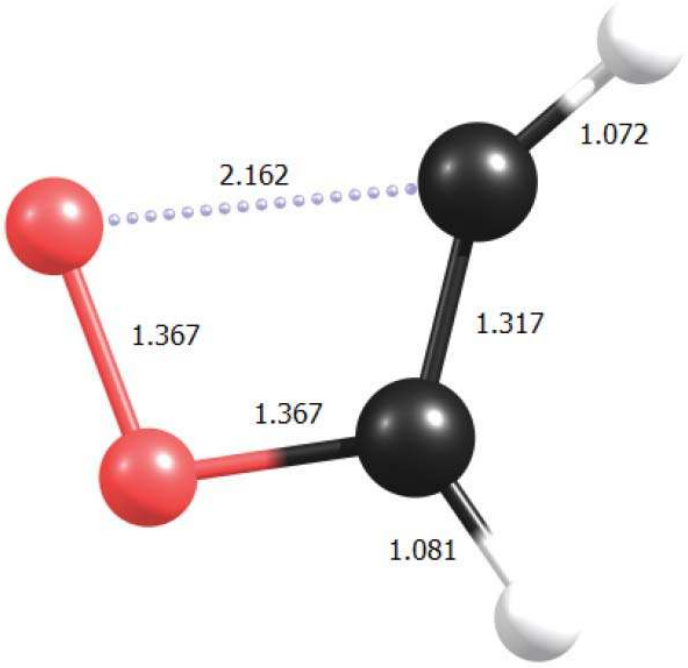

Figure 4: Geometry of the planar minimum energy crossing point for C_2H_2 + O_2 derived at the CCSD/aug-ccc-pVTZ level of theory. Bond lengths are in 10^{-10} m.

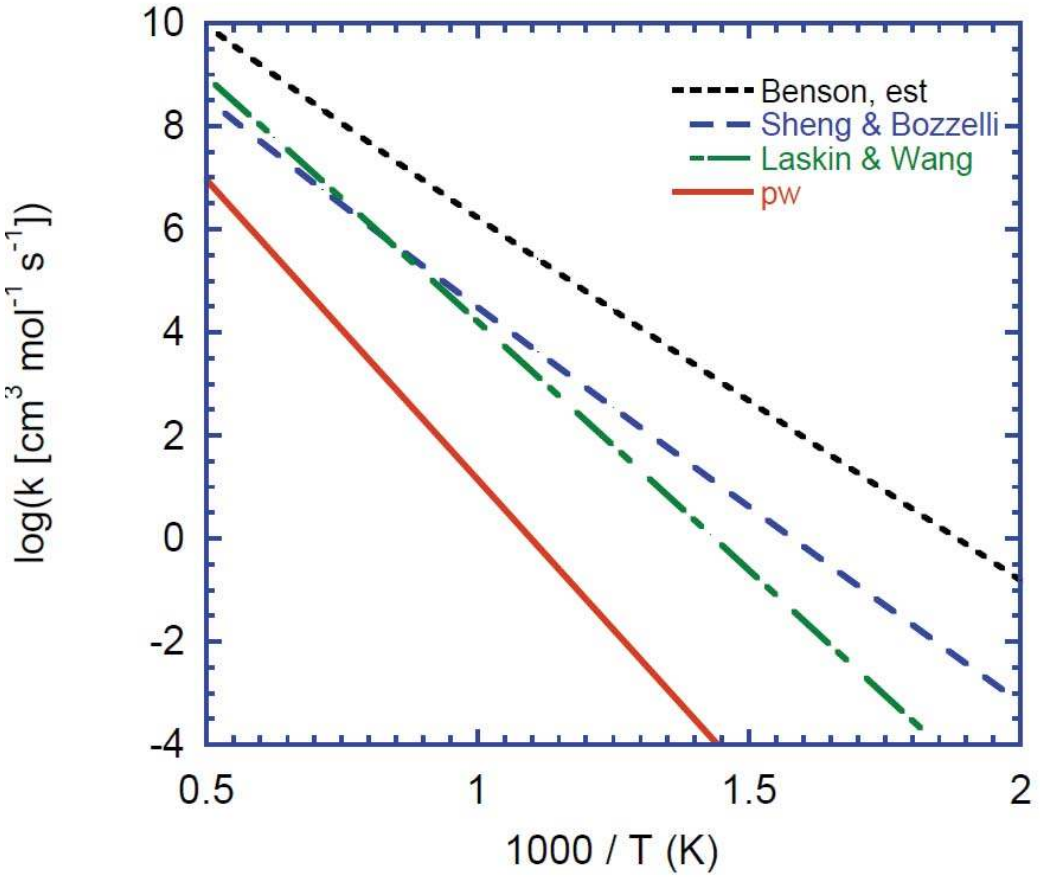

Figure 5: Arrhenius plot for the $C_2H_2 + O_2$ reaction. The rate constants are drawn from Benson [51] (with pre-exponential factor estimated by Glarborg et al. [42]); Sheng and Bozzelli [52], Laskin and Wang [50], and present work (pw). The value from Laskin and Wang is a composite rate constant for the sequence $C_2H_2 \rightleftarrows H_2CC$; $H_2CC + O_2 \rightarrow$ products, assuming the isomerization step to be partially equilibrated.

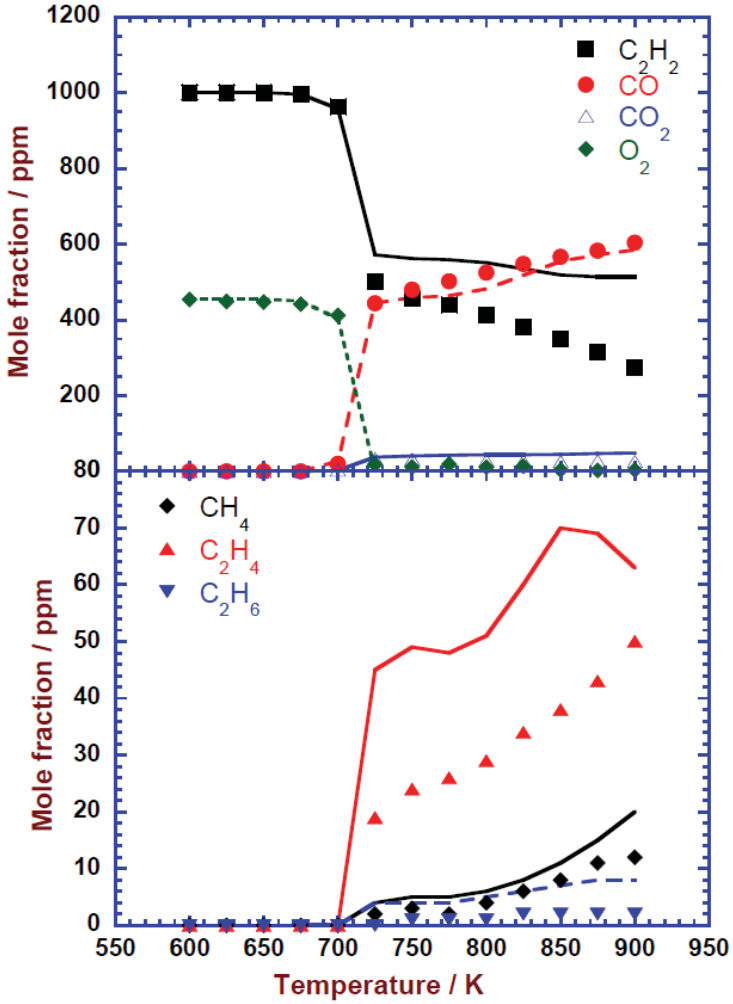

Figure 6: Comparison of experimental and predicted concentration profiles as a function of the reactor temperature for the reducing experiment with C_2H_2/O_2 ($\lambda = 0.18$). The pressure was 59.6 bar and the reactor residence time was 8792/T (s·K). The inlet composition was 1000 ppm C_2H_2, 455 ppm O_2, and N_2 by difference. The symbols mark experimental data while solid lines denote model predictions obtained at isothermal conditions.

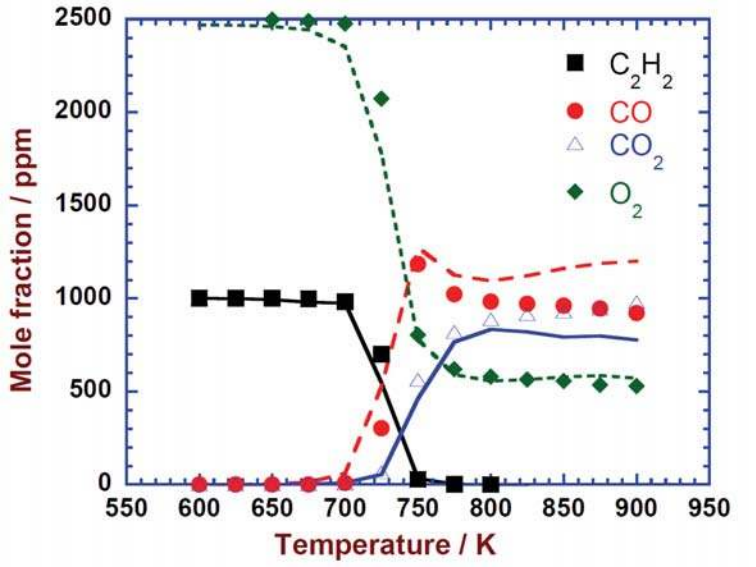

Figure 7: Comparison of experimental and predicted concentration profiles as a function of the reactor temperature for the stoichiometric experiment with C_2H_2/O_2 ($\lambda = 0.99$). The pressure was 59.6 bar and the reactor residence time was 8827/T (s·K). The inlet composition was 1000 ppm C_2H_2, 2470 ppm O_2, and N_2 by difference. The symbols mark experimental data while solid lines denote model predictions obtained at isothermal conditions.

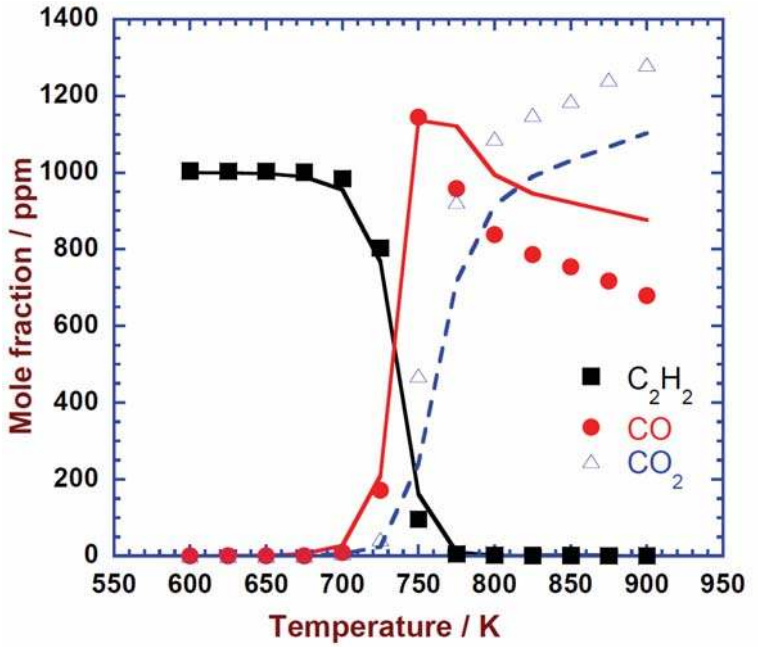

Figure 8: Comparison of experimental and predicted concentration profiles as a function of the reactor temperature for the oxidizing experiment with C_2H_2/O_2 ($\lambda = 19.4$). The pressure was 49.6 bar and the reactor residence time was 7346/T (s·K). The inlet composition was 1000 ppm C_2H_2, 4.9% O_2, and N_2 by difference. The symbols mark experimental data while solid lines denote model predictions obtained at isothermal conditions.

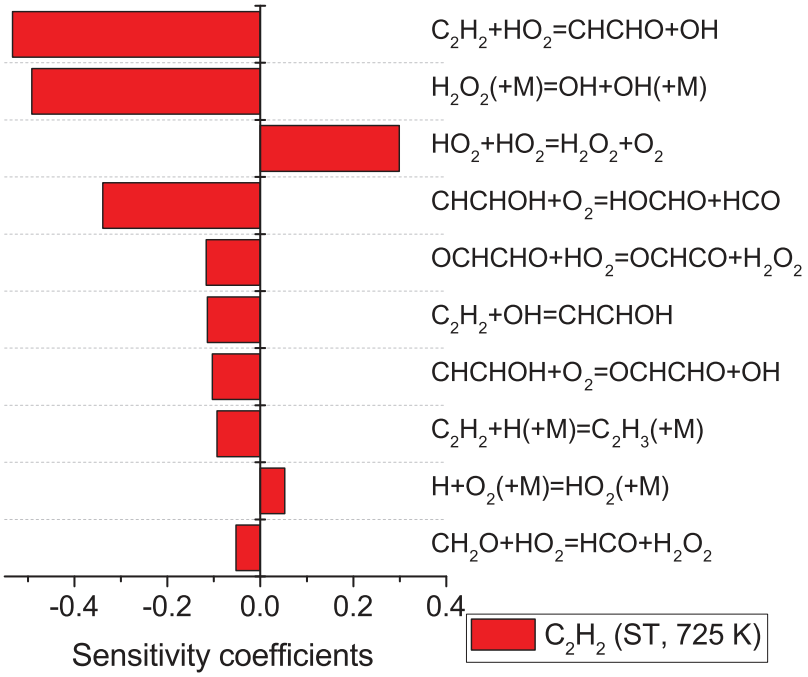

Figure 9: Sensitivity of the predicted C_2H_2 concentration for stoichiometric conditions (Fig. 7) at 725 K.

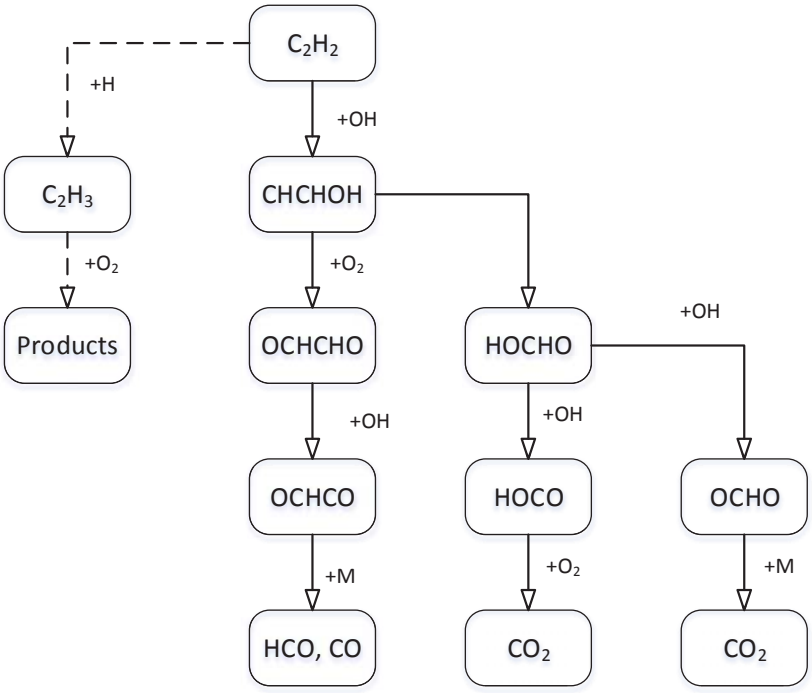

Figure 10: Main reaction pathways for C_2H_2 conversion at the investigated conditions. The solid lines denote pathways important over the range of stoichiometries investigated, while dashed lines denote pathways important only under reducing conditions.

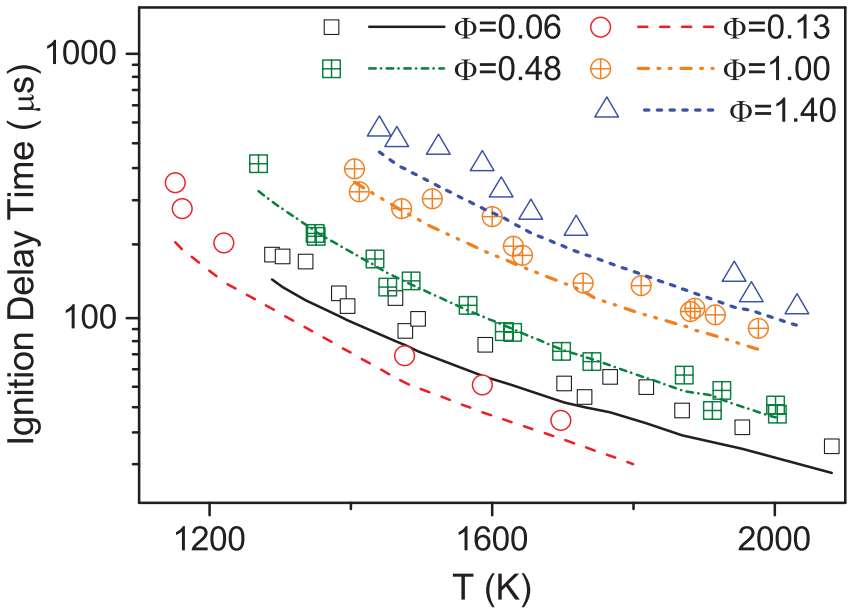

Figure 11: Ignition delay times of C_2H_2 at average pressure of 1.2 atm ($\pm$10%) at different stoichiometries. Inlet compositions (balance Ar): Φ = 0.063 (C_2H_2 = 0.25%; O_2 = 10%); Φ=0.125) (C_2H_2 = 0.5%; O_2 = 10%); Φ = 0.48 (C_2H_2 = 0.5%; O_2 = 2.6%); Φ = 1.0 (C_2H_2 = 0.5%; O_2 = 1.25%); Φ = 1.4 (C_2H_2 = 0.5%; O_2 = 0.89%). Symbols mark experimental results taken from Eiteneer and Frenklach [13] while lines denote modeling predictions at a fixed pressure of 1.2 atm. The ignition delay time was defined by the maximum of CO concentration.

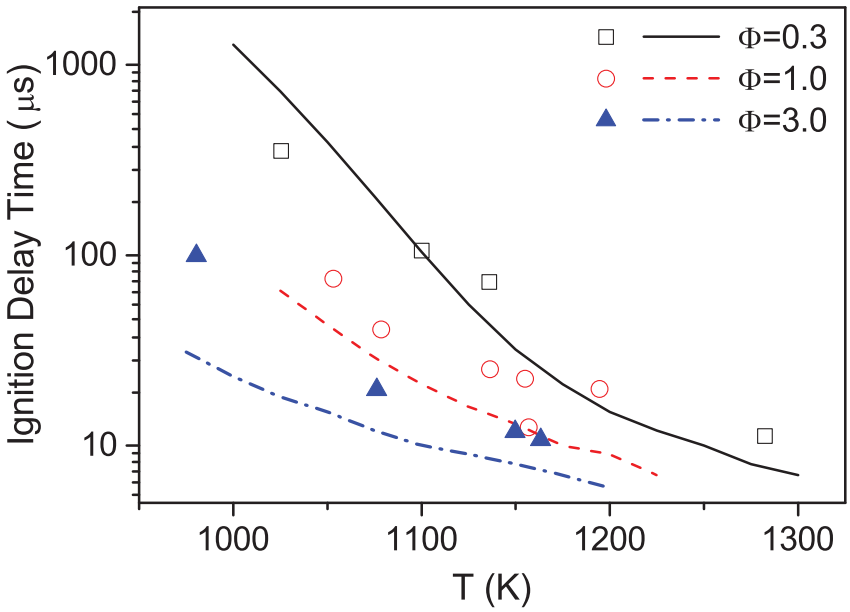

Figure 12: Ignition delay times of C_2H_2 at 6.5 bar under fuel-rich (Φ=3, 20.3% C_2H_2 + 16.7%O_2 in Ar), stoichiometric (Φ=1, 7.75% C_2H_2 + 19.38%O_2 in AR), and fuel-lean (Φ=0.3, 2.27% C_2H_2 + 20.4%O_2 in AR) conditions. Symbols mark experimental results taken from Tereza et al. [14] while lines denote modeling predictions. The ignition delay time was defined by the maximum temperature gradient.

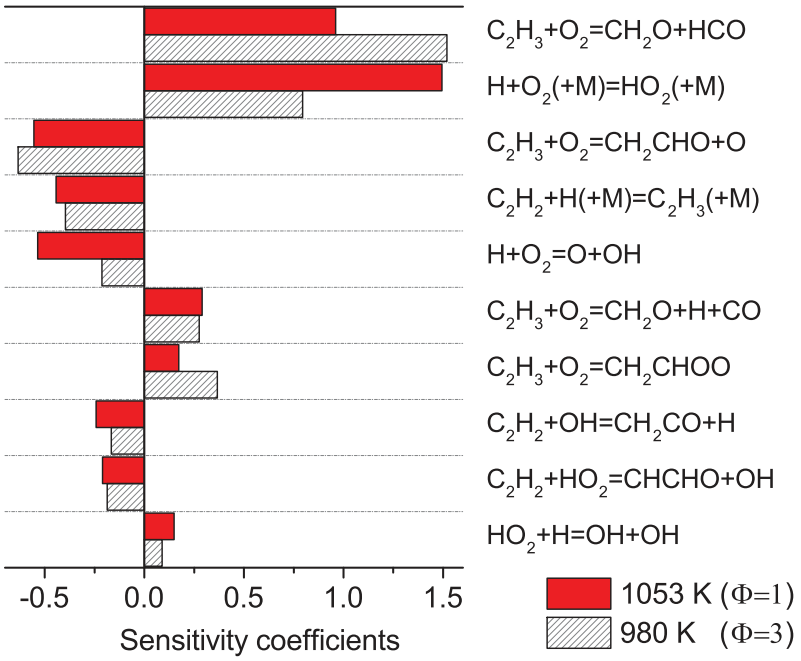

Figure 13: Sensitivity of ignition delay time of C_2H_2 at 1053 K (Φ=1) and 980 K (Φ=3) at 6.5 bar pressure. Other initial conditions are as those in fig. 12. The sensitivity coefficient is defined as $S_{\tau,i}=(\Delta\tau/\tau)$ / $(\Delta k_i/k_i)$ where τ and k_i present ignition delay time and reaction rate constants, respectively.

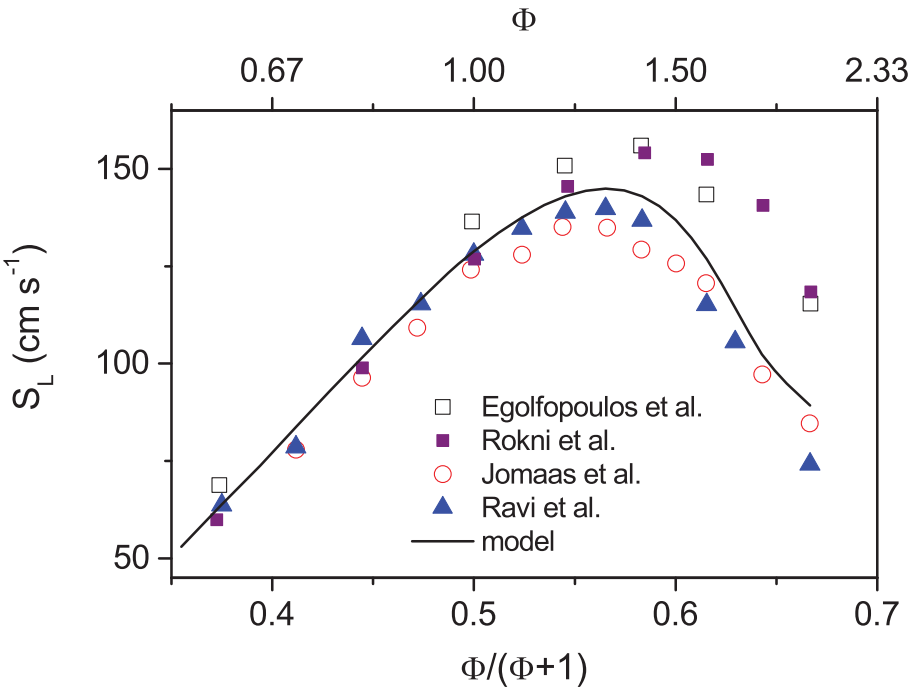

Figure 14: Laminar burning velocity of C_2H_2/air at 1 atm and initial temperature ~300 K. Symbols mark experimental results from Egolfopoulos et al. [24], Rokni et al. [29], Jomaas et al. [30], and Ravi et al. [31] while the solid line denotes the prediction of the present model.

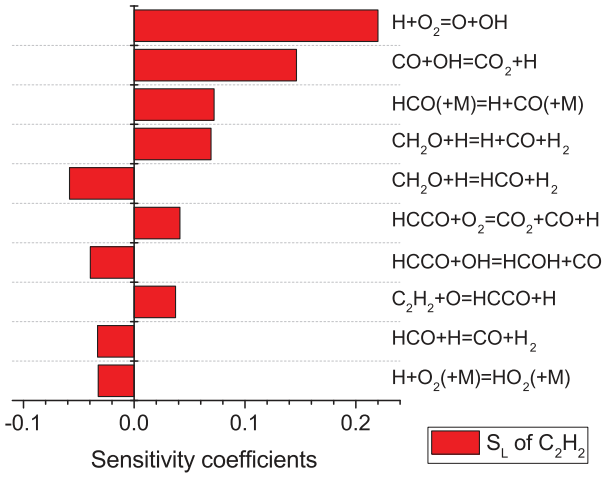

Figure 15: Sensitivity of laminar burning velocity of stoichiometric C_2H_2/air mixture at 1 atm and initial temperature ~300 K.

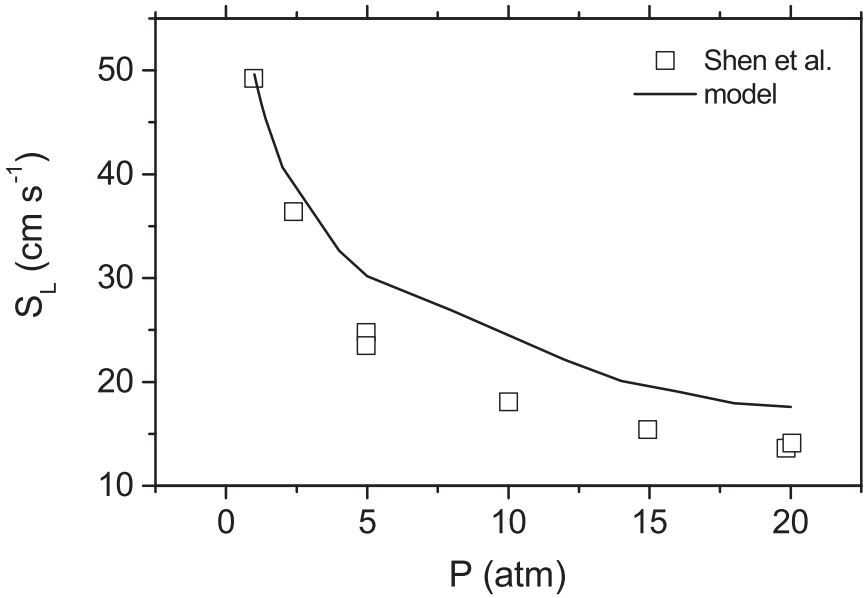

Figure 16: Laminar burning velocity versus pressure for a lean mixture of 3.4% C_2H_2, 10.6% O_2, 40% N_2 and 46% He at initial temperature of 298 K. Symbols mark experimental results from Shen et al. [32] while the solid line denotes modeling predictions.